

Multi-step approach to microscopic models for frustrated quantum magnets – the case of the natural mineral azurite – – Supplementary Material –

Harald Jeschke,¹ Ingo Opahle,¹ Hem Kandpal,² Roser Valentí,¹ Hena Das,³ Tanusri Saha-Dasgupta,³
Oleg Janson,⁴ Helge Rosner,⁴ Andreas Brühl,⁵ Bernd Wolf,⁵ Michael Lang,⁵ Johannes Richter,⁶
Shijie Hu,⁷ Xiaoqun Wang,⁷ Robert Peters,⁸ Thomas Pruschke,⁹ and Andreas Honecker⁹

¹*Institut für Theoretische Physik, Goethe-Universität Frankfurt am Main, 60438 Frankfurt am Main, Germany*

²*IFW Dresden, POB 270116, 01171 Dresden, Germany*

³*Satyandranath Bose National Centre for Basic Sciences, Kolkata 700098, India*

⁴*Max Planck Institute for Chemical Physics of Solids, 01187 Dresden, Germany*

⁵*Physikalisches Institut, Goethe-Universität Frankfurt am Main, 60438 Frankfurt am Main, Germany*

⁶*Institut für Theoretische Physik, Universität Magdeburg, P.O. Box 4120, 39016 Magdeburg, Germany*

⁷*Department of Physics, Renmin University of China, Beijing 100872, China*

⁸*Department of Physics, Graduate School of Science, Kyoto University, Kyoto 606-8502, Japan*

⁹*Institut für Theoretische Physik, Georg-August-Universität Göttingen, 37077 Göttingen, Germany*

(Dated: December 5, 2010; revised April 21, 2011)

SUPPLEMENTARY MATERIAL

S1. Density functional calculations

Structure relaxations were performed with the Car-Parrinello projector augmented wave (CP-PAW) method [1]. We employed a plane wave cutoff of 30 Ryd for the plane wave part and of 120 Ryd for the density, respectively, and we used the following sets of (s,p,d) projector functions per angular momentum: Cu(2,2,2), O(2,2,1), C(2,2,1) and H(2,0,0). We employed a $(4 \times 4 \times 4)$ k mesh and the $P21/c$ symmetry was preserved during the relaxation with the help of 60 constraints. The relaxation with the generalized gradient approximation (GGA) functional [2] resulted in small bond length changes of up to 4% and in angle changes up to 2° compared to the experimental data from Ref. [3].

The relative strengths of the exchange pathways in azurite have been obtained by using the electronic structure technique of muffin-tin orbital (MTO) based NMTO-downfolding [4, 5].

DFT calculations were performed with the full potential local orbital method [6] (FPLO), version 8.50, and the full potential augmented plane wave (FLAPW) method as implemented in the WIEN2k [7] code, which has been used to crosscheck the FPLO results for selected supercells. Total energies for different spin configurations were obtained in the GGA+U formalism, employing both the atomic limit (AL) as well as the around mean field (AMF) double counting correction. The AL double counting correction turned out to be the better choice for the calculation of a realistic set of model parameters for azurite because the ratios J_i/J_2 are strongly dependent on U in the case of the AMF double counting correction and can even adopt unphysical values ($J_1, J_3 > J_2$).

Table SI shows the complete set of exchange coupling parameters J_i , obtained with the FPLO code (version

U [eV]	J_1	J_2	J_3	J_4	J_5	J_6	J_7	J_m	J_d
4	34.1	145.4	35.4	5.9	2.9	16.2	-1.7	5.9	-1.7
6	21.3	82.8	21.2	3.8	1.5	8.6	-1.8	3.9	-0.8
8	13.5	42.8	12.5	2.7	0.6	4.4	-1.7	2.6	-0.4

TABLE SI. Exchange constants in K derived from FPLO GGA+U calculations with the atomic limit double counting correction. Slater parameters are chosen as $F_0 = U$, $F_2 = 8.6$ eV and $F_4 = 5.4$ eV, *i.e.*, $J_H = (F_2 + F_4)/14 = 1$ eV.

8.50) employing the GGA+U functional with atomic limit double counting correction. The calculations were repeated for three choices of the Coulomb correlation strength, $U = 4$ eV, 6 eV and 8 eV. The Hund's rule coupling J_H was chosen as $J_H = 1$ eV. The dominant coupling exhibits a proportionality to $1/U$. Note that the relative importance of the monomer-monomer coupling increases as U is increased.

J_2 is antiferromagnetic and the dominant interaction. One can therefore apply perturbative considerations in J_i/J_2 and argue that interchain excitations can be neglected to a first approximation (see Section S4). The essential items are that the interchain exchange constants J_4 to J_7 are small compared to J_2 and that they connect only to dimers of the neighboring chains (compare Figs. 1 (c) and (d)).

This suggests to reduce the set of interaction parameters to a minimal model including J_1 , J_2 , J_3 , and J_m only. In order to determine the effective values of these exchange constants quantitatively, we performed a least-square fit for the energy differences including only J_1 , J_2 , J_3 , and J_m in the model and set all other parameters to zero. It should be noted that the exchange constants obtained in this way are effective parameters, which contain the effect of the remaining parameters not included in the model as statistical average. Furthermore, it is also important that the procedure of statistical averaging is

U [eV]	J_1	J_2	J_3	J_m
4	50.5	151.1	35.7	3.4
6	30.0	85.4	21.0	3.0
8	17.9	43.9	12.0	2.4

TABLE SII. Effective exchange constants in K for a minimal model including only J_1 , J_2 , J_3 , and J_m obtained via statistical averaging (see text).

done over a sufficiently large manifold, since otherwise the effective parameters are to some degree arbitrary. The results are shown in Table SII. It can be seen that in the minimal model the effective parameters J_1 and J_3 show a strong asymmetry, which is not present in the full set of interaction parameters shown in Table SI. This is mainly due to integrating out of the fairly large coupling parameter J_6 in the model, which couples Cu monomer with Cu dimer atoms and in this way provides an effective asymmetry of J_1 and J_3 (inclusion of J_6 in addition to the minimal model again results in nearly identical J_1 and J_3 values).

S2. DMRG calculations

The theoretical magnetization curve in Fig. 3 (b) has been obtained with the static density-matrix renormalization group (DMRG) method [8, 9] using $m = 300$ states per block and four sweeps in each magnetization sector. The theory curves in Figs. 3 (c), 3 (d), and S1 have been obtained using transfer-matrix DMRG (TMRG [10, 11]) for the infinite system and $m = 300$. Note that these are in agreement with previous TMRG computations [12, 13] for the parameters of Ref. [14].

The transverse dynamic structure factor of Fig. 3 (e) has been computed by dynamic DMRG [15] for the parameters of Table I, line **3**, using open chains with $N = 60$ sites, up to $m = 200$ states per block and two sweeps per energy point. Note that for a meaningful comparison of scattering intensities with experiment, we had to take the precise positions of the copper atoms in azurite into account and use the same momentum perpendicular to the chain direction as in the experiment [16].

S3. Experiment

The specific heat of a plate-like azurite single crystal with the total mass of 0.36 mg was measured, employing an ac-calorimetry according to Ref. [17]. The data were taken in the temperature range $1.6 \text{ K} \leq T \leq 30 \text{ K}$ and in magnetic fields up to 8 T. The experiments were performed using a home-built AC-calorimeter especially designed for small plate-like samples. The sample holder, consisting of a resistive thermometer (Cernox CX-1080-

BG) and a heater, is attached to a ^4He -bath cryostat equipped with a superconducting magnet.

The magnetic susceptibility of azurite was measured in the temperature range between $2 \text{ K} \leq T \leq 300 \text{ K}$ and in magnetic fields up to $H = 4 \text{ T}$ using a Quantum Design SQUID magnetometer. The orientation of the single crystal (mass 55.26 mg) with respect to the external field was $H \perp b$ -axis. The data were corrected for the temperature-independent diamagnetic core contribution, according to Ref. [18] and the magnetic contribution of the sample holder. The latter was determined from an independent measurement.

S4. Perturbative treatment of interchain coupling

For a large and antiferromagnetic J_2 , one can use perturbative arguments to integrate out the copper dimers and generate effective interactions between the monomer copper atoms. In the limit of infinite J_2 , the two spins on the corresponding dimer bond are in their singlet state $\frac{1}{\sqrt{2}} (|\uparrow\downarrow\rangle - |\downarrow\uparrow\rangle)$. In this limit, the only interaction between the monomer spins is J_m . However, one can use degenerate perturbation theory in J_i/J_2 to generate further interactions between the monomer spins.

The second-order contribution to the monomer-monomer interactions within a chain is known [19] to be given by

$$\tilde{J}_m = \frac{(J_1 - J_3)^2}{2J_2}. \quad (1)$$

This effective interaction enhances the bare interaction J_m between the monomers along the chain provided that $J_1 \neq J_3$.

The interactions J_4 and J_7 connect dimers of neighboring chains (see Fig. 1 (d)). Accordingly, they contribute to interchain monomer-monomer exchange only in third order in perturbation theory and generate exchanges $\propto J_1^2 J_4/J_2^2$, $J_1 J_3 J_4/J_2^2$, $J_1^2 J_7/J_2^2$ and $J_1 J_3 J_7/J_2^2$. Using the values of the J_i in Table I, line **1**, these effective interchain exchanges are estimated to be at most on the order of $0.3 \text{ K} \approx J_m/10$ and thus can be neglected safely.

By contrast, J_5 and J_6 contribute in second order perturbation theory to interchain coupling since they connect dimers with monomers of the neighboring chains (see Fig. 1 (c)). The contribution from J_5 is given by $(J_1 + J_3) J_5/(2J_2)$. Inserting the numbers from Table I, line **1**, this again turns out to be on the order of $0.2 \text{ K} \approx J_m/10$, *i.e.*, also J_5 is sufficiently small to be neglected safely.

The exchange constant J_6 also contributes terms proportional to $J_1 J_6/J_2$ and $J_3 J_6/J_2$ to interchain effective monomer-monomer coupling. Inserting again the values of J_1 , J_2 , J_3 , and J_6 in Table I, line **1** into the second-order expression, we now obtain a contribution

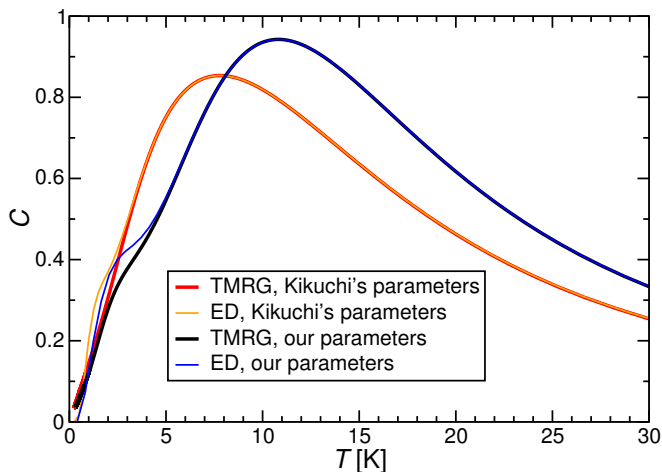


FIG. S1. TMRG and ED results for the zero-field specific heat per spin. The ED computations were performed for $N = 18$ spins. We show results both for our new parameter set, Table I, line **3**, as well as for Kikuchi's original parameter set Table I, line **4** $J_1 = 19$ K, $J_2 = 24$ K, $J_3 = 8.6$ K, and $J_m = 0$ [14].

on the order of 1.4 K $\approx J_m/2$ to the effective interchain monomer-monomer coupling. On the one hand, this is still sufficiently small not to give rise to relevant dispersion of the excitations perpendicular to the chains, in agreement with inelastic neutron scattering on azurite [16]. On the other hand, this value is too large to neglect J_6 completely.

In fact, in a mean-field picture, the monomer moments influence the effective monomer-monomer exchange along the neighboring chains. The reason is that the interchain couplings connect the monomer spins only to one of the dimer spins on the neighboring chains, thus breaking the symmetry of the exchange process along the chains and giving rise to corrections to (1). In this mean-field picture, the interchain coupling J_6 has the same effect as the intrachain coupling J_1 .

These arguments suggest that one may go from the full three-dimensional model to an effective chain model by neglecting J_4 , J_5 , and J_7 , and adding J_6 to J_1 . The difference between lines **1** and **2** of Table I or Tables SI and SII can indeed be understood at least qualitatively in this way although the reduction has been performed in a completely different manner.

S5. Specific heat

Experimentally, two anomalies have been observed in the magnetic specific heat at $T \approx 18$ K [14] and $T \approx 4$ K [14, 16] (compare also top panel of Fig. 3 (d)). Fig. S1 shows TMRG results for the specific heat per spin C in zero magnetic field. For our new parameter set, Ta-

N	monomer $\langle S_i^z \rangle$	dimer $\langle S_i^z \rangle$
18	0.47342867	0.01328567
24	0.47343148	0.01328426
30	0.47343154	0.01328423
36	0.47343154	0.01328423

TABLE SIII. Structure of the $M = 1/3$ plateau state for rings with N sites and the parameters in line **3** of Table I.

ble I, line **3** (black line in Fig. S1), we find a maximum of C at a temperature slightly above 10 K and a low-temperature feature at $T \approx 3$ K. Although this does not reproduce the experimental temperatures exactly, it is in better agreement with the experimental findings than the results for the original parameter set of Ref. [14] (red line in Fig. S1).

Fig. S1 includes exact diagonalization (ED) results for rings with $N = 18$ spins. We observe that finite-size effects have no visible effect for $T \gtrsim 6$ K.

S6. Structure of the 1/3 plateau

The $1/3$ plateau state of azurite has been characterized using NMR [20], which amounts to a measurement of the expectation values $\langle S_i^z \rangle$. This NMR study showed that the dimer spins are essentially in their singlet state with just 10% spin polarization on the dimers. Correspondingly, the monomer spins are almost polarized on the $1/3$ plateau.

Using ED for rings with $N = 18, 24, 30$, and 36 sites and our parameters line **3** of Table I, we find the structure of the $M = 1/3$ plateau state presented in Table SIII. We observe that the numerical results for the expectation values converge rapidly with system size and read off that the dimer spins are about 2.7% polarized each. This is only slightly smaller than the 10% observed in Ref. [20]. We note that the NMR experiment [20] involved a rotation around the crystallographic a -axis and speculate that this gives rise to non-commuting fields which enhance the dimer polarization as compared to the ideal Heisenberg model.

S7. Excitation spectrum on the 1/3 plateau

The excitation spectrum above the $1/3$ plateau of azurite has been probed by inelastic neutron scattering at $H = 14$ T [16]. These experiments observed two cosine-like bands of magnetic excitations with a minimum energy at the antiferromagnetic wave vector $k = \pi$. The two bands are sketched by the dashed lines in Figs. S2–S6. They are centered around ≈ 1.3 meV and ≈ 2.35 meV and have a width of 20.2 K and 3.6 K,

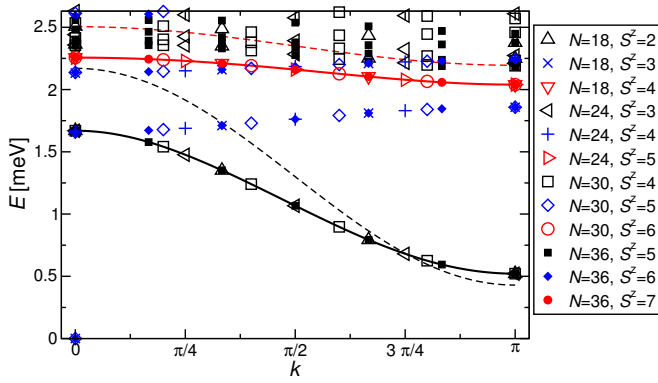


FIG. S2. Excitation spectrum at $H = 14$ T as computed by exact diagonalization with the parameters in Table I, line **3**. Solid black (red) lines connect the lowest excitations with spin quantum numbers smaller (larger) by one than that of the $1/3$ plateau state. Dashed lines indicate the location of the experimental result [16] for the corresponding excitations.

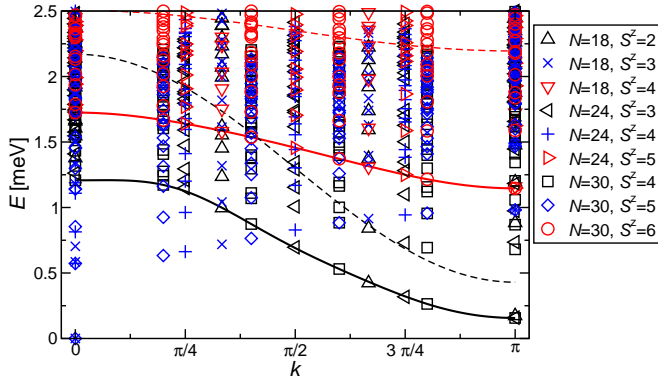


FIG. S3. Same as Fig. S2, but for Kikuchi's original parameter set Table I, line 4, $J_1 = 19$ K, $J_2 = 24$ K, $J_3 = 8.6$ K, and $J_m = 0$ [14].

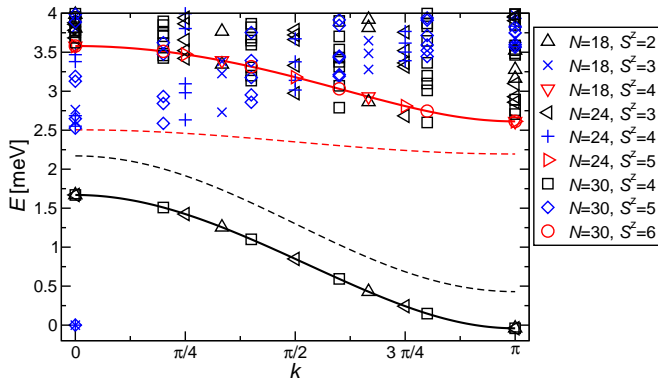


FIG. S4. Same as Fig. S2, but for the parameter set of Gu and Su [12, 13]: $J_1 = 23$ K, $J_2 = 43.7$ K, $J_3 = -9.3$ K, and $J_m = 0$.

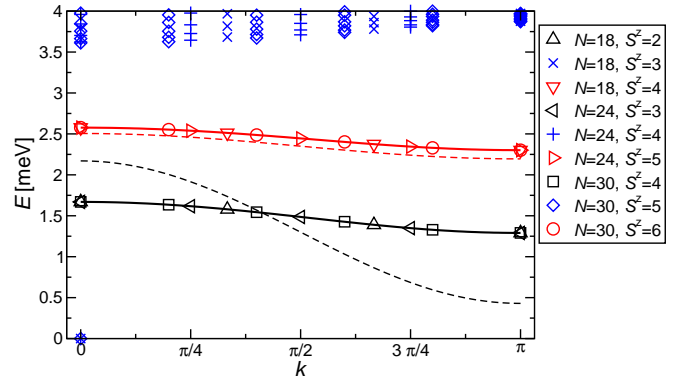


FIG. S5. Same as Fig. S2, but for a first parameter set proposed in Ref. [16]: $J_1 = 1$ K, $J_2 = 55$ K, $J_3 = -20$ K, and $J_m = 0$.

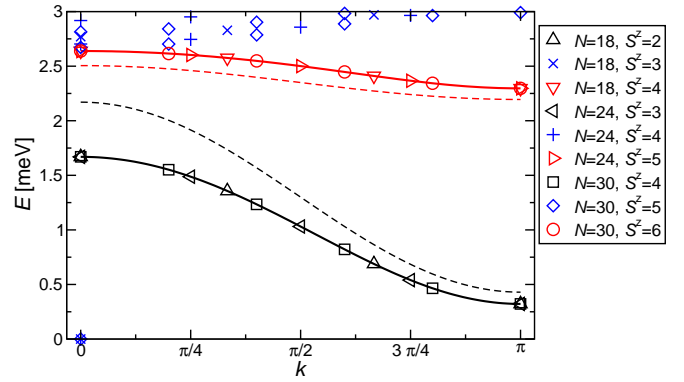


FIG. S6. Same as Fig. S2, but for the second parameter set proposed in Ref. [16]: $J_1 = 1$ K, $J_2 = 55$ K, $J_3 = -20$ K, and $J_m = 6.5$ K.

respectively. In particular the ratio of the bandwidths of the upper and lower bands is $1.8/10.1 \approx 1/5.6$.

Figs. S2–S6 show the excitation spectrum as a function of momentum k along the chain direction on the $1/3$ plateau computed by exact diagonalization with periodic boundary conditions. Black, blue, and red symbols correspond to excitations with $\Delta S^z = -1, 0$, and 1 , respectively. The blue symbol at $k = 0$ and energy $E = 0$ corresponds to the ground state of the $1/3$ plateau. A Fourier analysis of the lowest $\Delta S^z = \pm 1$ excitations for $N = 30$ sites yields the solid lines in Figs. S2–S6. One observes that the lowest $\Delta S^z = \pm 1$ excitations collapse onto these lines for all sizes N , demonstrating that the main effect of a finite system size N on these excitations is a discretization of the allowed values of the momentum k (see also [21]).

First let us look at our final parameter set Table I, line **3**. The lowest black and red excitation in Fig. S2, *i.e.*, the two solid curves correspond to the two dispersion curves already observed in Fig. 3 (e). Note that energy and mo-

momentum resolution in Fig. 3 (e) is essentially limited by the open ends of the finite-size chains which were used for the dynamic DMRG computations. Evidently, inspection of the momentum-resolved bare energy levels shown in Fig. S2 yields better energy-momentum resolution at the expense of losing information about the neutron intensities of the excitations. Indeed, in Fig. S2 we see a large number of excitations at energies above 2 meV and only the dynamic structure factor of Fig. 3 (e) shows that they have very little contribution to the inelastic neutron cross section. From the bare energy levels of Fig. S2, we read off a bandwidth ratio of $1/5.3$ which is very close to the experimental value [16].

Fig. S3 shows the expected excitation spectrum for Kikuchi's original parameter set Table I, line 4 [14]. Note that we have computed only the 20 lowest excitations in some sectors for $N \geq 24$ and that the density of states is already quite large at energies above 1 meV in the present case. Hence, some levels may be missing in Fig. S3 at energies $E > 2$ meV for $S^z \leq N/6$ and $N \geq 24$. We nevertheless keep this region in order to be able to show the location of the excitations observed by inelastic neutron scattering on azurite [16] (dashed lines). In the present case it is not so easy to distinguish two cosine-like bands in the numerical results. If one uses the lowest black and red energy level, respectively, one finds a bandwidth ratio close to $1/1.9$, quite far off the experimental result [16].

Further proposals of parameter sets [12, 13, 16] contain a ferromagnetic J_3 . Ref. [22] already pointed out that a ferromagnetic J_3 is hard to reconcile with the crystal structure of azurite given the $d_{x^2-y^2}$ character of the relevant copper orbitals. We will nevertheless look at the excitation spectra for these parameter sets and demonstrate that they are either inconsistent or at least yield less good agreement with the neutron scattering experiments [16] than our final parameter set given in Table I, line 3.

The parameter set of Gu and Su [12, 13] $J_1 = 23$ K, $J_2 = 43.7$ K, $J_3^{xy} = -6.9$ K, $J_3^z = -11.73$ K, $J_m = 0$ has an artificially large magnetic anisotropy in the supposedly ferromagnetic J_3 . Replacing this by an average value $J_3 = -9.3$ K, we find the excitation spectrum shown in Fig. S4. Not only is the bandwidth ratio of approximately $1/1.8$ again far away from the experimental result [16], but in this case the upper excitation branch is about 1 meV (≈ 10 K) too high in energy.

Finally, Ref. [16] tried to invert perturbative results for the effective monomer-monomer and dimer-dimer exchanges along the chain in order to propose $J_1 = 1$ K, $J_2 = 55$ K and a ferromagnetic $J_3 = -20$ K. We discuss two variants of these parameters, starting in Fig. S5 with $J_m = 0$. In this case, we find a bandwidth ratio $1/1.4$ which is clearly inconsistent with the experimental result. However, it was already proposed in Ref. [16] to improve this behavior by adding a $J_m = 6.5$ K. The result with such a J_m included is shown in Fig. S6. While

inclusion of $J_m = 6.5$ K improves the agreement with experiment [16], the result is not quite as good for our final parameter set Table I, line 3. In particular, the bandwidth ratio is just $1/4$.

To summarize the discussion of this subsection, we have demonstrated that our final parameter set Table I, line 3 yields the best agreement with inelastic neutron scattering on the $1/3$ plateau [16] among the proposals of Refs. [12–14, 16]. In particular, inelastic neutron scattering is inconsistent with the parameters proposed in Refs. [12–14].

S8. Perspectives

There are some further refinements of the model for azurite to be implemented in future investigations. Firstly, we have argued interchain coupling to be unimportant for a basic description of azurite, but, although small, it is present and likely to be responsible for the following features: (i) The strong curvature at the lower edge of $1/3$ plateau in the theoretical magnetization curve of Fig. 3 (b) versus the smoother behavior observed in the experiment for $H \perp b$ is characteristic for one- versus higher-dimensional physics [23–25]. (ii) An ordering transition at temperatures slightly below 2 K [14, 26, 27] is evident in Fig. 3 (d), *i.e.*, interchain coupling affects thermodynamic properties at temperatures of a few Kelvin. In view of the success of the effective one-dimensional model Table I, line 3, we are confident that our prediction of Table I, line 1 for the exchange ratios of the full three-dimensional model is also reliable. Indeed, it would be very interesting to compare the predictions of this three-dimensional model for the zero-field ordered state with the corresponding recent experimental observations [28]. However, this will require very different methods from the present work and thus is an interesting topic for future investigations.

Secondly, we have neglected magnetic anisotropy in the theoretical model although experiments [14] show that it is present in azurite and affects magnetic properties for a magnetic field parallel to the crystallographic b -axis at an energy scale of a few Kelvin.

Finally, we would like to emphasize that we find all J_i antiferromagnetic with similar values of J_1 and J_3 , thus placing azurite in a highly frustrated parameter regime. This is reflected by the almost localized nature of the dimer excitations. These excitations will become low-energy excitations in magnetic fields around 32 T, and one expects related unusual thermodynamic behavior like an enhanced magnetocaloric effect [29, 30]. This calls for additional thermodynamic measurements close to the saturation field of azurite.

-
- [1] P. E. Blöchl, Phys. Rev. B **50**, 17953 (1994).
- [2] J. P. Perdew, K. Burke, and M. Ernzerhof, Phys. Rev. Lett. **77**, 3865 (1996).
- [3] F. Zigan and H. D. Schuster, Z. Kristallogr. **135**, 416 (1972).
- [4] O. K. Andersen and T. Saha-Dasgupta, Phys. Rev. B **62**, R16219 (2000).
- [5] O. K. Andersen, T. Saha-Dasgupta, and S. Ezhov, Bull. Mater. Sci. **26**, 19 (2003).
- [6] K. Koepnik and H. Eschrig, Phys. Rev. B **59**, 1743 (1999); <http://www.FPL0.de>.
- [7] P. Blaha, K. Schwarz, C. Madsen, D. Kvasnicka, and J. Luitz, *WIEN2k: An augmented plane wave plus local orbitals program for calculating crystal properties*. (TU Wien, Austria, 2001).
- [8] S. R. White, Phys. Rev. Lett. **69**, 2863 (1992).
- [9] U. Schollwöck, Rev. Mod. Phys. **77**, 259 (2005).
- [10] R. J. Bursill, T. Xiang, and G. A. Gehring, J. Phys.: Condens. Matter **8**, L583 (1996).
- [11] X. Wang and T. Xiang, Phys. Rev. B **56**, 5061 (1997).
- [12] B. Gu and G. Su, Phys. Rev. Lett. **97**, 089701 (2006).
- [13] B. Gu and G. Su, Phys. Rev. B **75**, 174437 (2007).
- [14] H. Kikuchi, Y. Fujii, M. Chiba, S. Mitsudo, T. Idehara, T. Tonegawa, K. Okamoto, T. Sakai, T. Kuwai, and H. Ohta, Phys. Rev. Lett. **94**, 227201 (2005).
- [15] E. Jeckelmann, Phys. Rev. B **66**, 045114 (2002).
- [16] K. C. Rule, A. U. B. Wolter, S. Süllow, D. A. Tennant, A. Brühl, S. Köhler, B. Wolf, M. Lang, and J. Schreuer, Phys. Rev. Lett. **100**, 117202 (2008).
- [17] P. F. Sullivan and G. Seidel, Phys. Rev. **173**, 679 (1968).
- [18] O. Kahn, *Molecular Magnetism*. (Wiley-VCH, New York, 1993).
- [19] A. Honecker and A. Läuchli, Phys. Rev. B **63**, 174407 (2001).
- [20] F. Aimo, S. Krämer, M. Klanjšek, M. Horvatić, C. Berthier, and H. Kikuchi, Phys. Rev. Lett. **102**, 127205 (2009).
- [21] H.-J. Mikeska and C. Luckmann, Phys. Rev. B **77**, 054405 (2008).
- [22] J. Kang, C. Lee, R. K. Kremer, and M.-H. Whangbo, J. Phys.: Condens. Matter **21**, 392201 (2009).
- [23] G. I. Dzhaparidze and G. I. Nersesyan, JETP Lett. **27**, 334 (1978).
- [24] V. L. Pokrovsky and A. L. Talapov, Phys. Rev. Lett. **42**, 65 (1979).
- [25] E. G. Batyev and L. S. Braginskii, Soviet Physics JETP **60**, 781 (1984).
- [26] H. Forst, G. Taylor, and R. B. King, J. Chem. Phys. **31**, 929 (1959).
- [27] M. C. R. Gibson, K. C. Rule, A. U. B. Wolter, J.-U. Hoffmann, O. Prokhnenko, D. A. Tennant, S. Gerischer, M. Kraken, F. J. Litterst, S. Süllow, J. Schreuer, H. Luetkens, A. Brühl, B. Wolf, and M. Lang, Phys. Rev. B **81**, 140406(R) (2010).
- [28] K. C. Rule, M. Reehuis, M. C. R. Gibson, B. Ouladdiaf, M. J. Gutmann, J.-U. Hoffmann, S. Gerischer, D. A. Tennant, S. Süllow, and M. Lang, Phys. Rev. B **83**, 104401 (2011).
- [29] O. Derzhko, J. Richter, A. Honecker, and H.-J. Schmidt, Low Temp. Phys. **33**, 745 (2007).
- [30] A. Honecker, S. Hu, R. Peters, and J. Richter, J. Phys.: Condens. Matter **23**, 164211 (2011).